climate

MDPI

Article

A Comprehensive AI Approach for Monitoring and Forecasting Medicanes Development

Javier Martinez-Amaya [1,*], Veronica Nieves [1,*] and Jordi Muñoz-Mari [2]

[1] Image Processing Laboratory, University of Valencia, 46980 Valencia, Spain
[2] School of Engineering, University of Valencia, 46100 Valencia, Spain; jordi.munoz@uv.es
* Correspondence: javier.martinez-amaya@uv.es (J.M.-A.); veronica.nieves@uv.es (V.N.)

Abstract: Medicanes are rare cyclones in the Mediterranean Sea, with intensifying trends partly attributed to climate change. Despite progress, challenges persist in understanding and predicting these storms due to limited historical tracking data and their infrequent occurrence, which make monitoring and forecasting difficult. In response to this issue, we present an AI-based system for tracking and forecasting Medicanes, employing machine learning techniques to identify cyclone positions and key evolving spatio-temporal structural features of the cloud system that are associated with their intensification and potential extreme development. While the forecasting model currently operates with limited training data, it can predict extreme Medicane events up to two days in advance, with precision rates ranging from 65% to 80%. These innovative data-driven methods for tracking and forecasting provide a foundation for refining AI models and enhancing our ability to respond effectively to such events.

Keywords: extreme events; Medicanes; tropical cyclones; Mediterranean Sea; machine learning; artificial intelligence prediction; tracking

Citation: Martinez-Amaya, J.; Nieves, V.; Muñoz-Mari, J. A Comprehensive AI Approach for Monitoring and Forecasting Medicanes Development. *Climate* **2024**, *12*, 220. https://doi.org/10.3390/cli12120220

Academic Editor: Antonello Pasini

Received: 14 November 2024
Revised: 10 December 2024
Accepted: 11 December 2024
Published: 13 December 2024

1. Introduction

The escalation in the intensity of extreme weather events has emerged as a pressing concern, with tropical cyclones (TCs) ranking among the most destructive natural phenomena increasingly influenced by climate change and global warming [1,2]. While these storms typically develop in tropical regions, there exists a unique category of cyclone that forms over the Mediterranean Sea, known as Medicanes [3–5]. Over the past years, various studies have examined and reported on these phenomena, highlighting their inherent risk [4–10]. Considering the densely populated areas surrounding the Mediterranean and future projections indicating the intensification of Medicanes in forthcoming years [11–13], precise monitoring and forecasting of their development have assumed paramount importance.

While the precise definition of Mediterranean Hurricanes is still debated, these systems share several characteristics with TCs [14,15]. Medicanes are generally distinguished by their tropical-like structure, including the presence of a warm core, a circular eye surrounded by a convective eyewall, and a roughly axisymmetric cloud pattern, as noted in studies on their climatology [16–18]. However, the absence of a precise and widely agreed-upon definition complicates their identification. This lack of clarity poses significant challenges in building comprehensive tracking databases for Medicanes, as the difficulty stems not only from defining their unique characteristics but also from the absence of standardized tracking methodologies [15]. Addressing these gaps is a critical aspect of the present study, which aims to establish a robust framework for Medicane identification and support the development of consistent tracking databases. Existing methods are often based on different characteristics of Medicanes and case studies [4,9,10,19–21], making direct comparisons impractical and likely inconclusive without a standardized benchmark [22]. This study provides a foundation for future research to evaluate and refine these methods under unified conditions.

Furthermore, existing forecasting models primarily rely on computationally intensive numerical simulations [23], which often struggle to accurately capture the nonlinear and extreme development of Medicanes [7], among other challenges [14,15]. As emphasized in the work by Flaounas et al. [14], there is a growing recognition that novel sensitivity calculation methods should account for the nonlinear connections between predictions and predictors [24]. Advancements in artificial intelligence (AI) and machine learning (ML) techniques offer innovative avenues for addressing the challenges posed by climate change, especially in tracking and forecasting extreme weather events [14,19,25]. However, to date, no machine learning model has been specifically designed for predicting events like Medicanes. This study also addresses this gap by developing a customized forecasting tool for predicting Medicanes, leveraging AI to explore these emerging capabilities.

Therefore, to address these challenges, we must confront several primary issues: (1) The absence of a comprehensive database that consolidates information related to cyclone location and associated features (e.g., wind speed or central pressure), as well as the lack of a standardized tracking algorithm dedicated to Medicanes [18]; (2) numerical forecasting models that are not adequately equipped to handle with the complexities of nonlinear and extreme events, especially those characterized by rapid intensification, due to the inherent approximations and parametrizations required for such processes, limited model resolution, inaccurate initial conditions, and the difficulty in resolving interactions with larger-scale systems and boundary conditions [5–7,26,27]; and (3) insufficient historical monitoring and the limited number of past events, resulting in a scarcity of data [12]. To overcome these challenges, we developed an AI-driven methodology designed to track and predict Medicanes, including those with rapid development: (1) A machine learning-based tracking methodology using a k-means algorithm, offering improved adaptability to data patterns amidst changing climatic conditions and reducing dependency on predefined thresholds (spatial or atmospheric pressure-based criteria) commonly used in traditional models, which often struggle to capture the variability and complexity of Medicane tracks [15]; and (2) a machine learning prediction framework for Medicane forecasting, adapted from the work of Martinez-Amaya et al. [25], which combines Convolutional Neural Networks (CNNs) and Random Forest (RF) models. This approach enhances capacity to capture complex, nonlinear relationships in the data—capabilities that traditional numerical models, with their reliance on simplified parameterizations, often lack, particularly when forecasting rapid intensification events. This resource-efficient and adaptable data-driven alternative, originally developed for TCs in the Pacific and Atlantic oceans and now tailored to address the unique characteristics of Medicanes enables effective forecasting in contexts where computational efficiency and adaptability are crucial. Given the binary nature of forecasting extreme events using RF models, where outcomes are either accurately predicted or missed, this study provides an inherently reliable approach to Medicane forecasting, with each prediction validated against documented events.

K-means, a widely adopted unsupervised clustering technique for storm pattern detection [28,29], is used to track cyclone positions by processing mean sea level pressure maps through an automated grid search approach. This enables us to determine the center coordinates of each storm throughout its lifetime, a crucial step for obtaining the associated wind speed. Additionally, we leverage CNNs, which are deep learning algorithms capable of automatically extracting relevant spatial structural characteristics from satellite imagery of the cyclone cloud's system [25]. These features, closely linked to the intensification of extreme events, enhance the accuracy of predicting the storm's peak stage [25,30,31]. Note that the structural predictors, though indirect, inherently reflect changes in the physical processes driving storm intensification (see, e.g., [32,33]). Then, RF, an ensemble learning algorithm that combines multiple decision trees for robust predictions, is trained using the full range of spatio-temporal structural information and intensity levels (wind speed) of these events. This AI-based approach, which enables the exploration of optimal combinations of the nonlinearly linked variables for predicting extreme Medicane development, is intrinsically validated against real-world data, offering a reliable means to assess its

accuracy. While traditional comparisons against other methods could not be performed due to the distinct structure of the RF approach—where outcomes are clearly dichotomized as either correctly forecasted or not—our results indicate that the precision achieved aligns well with observed occurrences, underscoring the model's robustness in forecasting Medicanes. Our predictions span multiple lead-time (6 to 36 h), enabling forecasters to provide advance notice before the Medicane reaches its peak intensity and potentially destructiveness. This system facilitates structured and timely delivery of information for preparedness and response efforts.

2. Materials and Methods

2.1. Data Products

In this section, we present an array of data products derived from a combination of reanalysis and remote sensing data. Our investigation into Medicanes monitoring and forecasting involves leveraging these two complementary sources of information. Reanalysis data offer a comprehensive and consistent record of historical atmospheric conditions, while remote sensing data provide high-resolution spatial coverage, enabling a detailed understanding of the storm structural changes linked to their intensification.

2.1.1. Atmospheric Reanalysis Data

The Copernicus European Regional ReAnalysis (CERRA) dataset encompasses subdaily data for Mean Sea Level Pressure (MSLP) and Wind Speed (WS) at 10 m above the surface throughout 2020. This dataset offers a spatial resolution of 5.5 km at 3-hour intervals [34] and was collected from 1984 to 2020, focusing on the Mediterranean basin, as defined by geographic coordinates ([−5° 35° E], [20° 45° N]). Since CERRA data are only available up to 2020, we transitioned to using the hourly ECMWF Reanalysis v5 (ERA-5) dataset from 2021 onward, which provides a global resolution of approximately 31 km [35]. Despite the coarser spatial resolution of ERA-5, our experiments demonstrated that incorporating this product allowed the inclusion of additional Medicane cases, thereby improving model performance in forecasting analysis. This was particularly valuable given the limited number of events in the Mediterranean region. However, using only ERA-5 for the entire analysis period was not feasible due to its spatial resolution limitations, which hinder effective tracking of cyclone trajectories. Data are provided by the Copernicus Climate Change Service (C3S) Climate Data Store (https://cds.climate.copernicus.eu/, accessed on 30 November 2023).

A critical step in identifying Medicanes is detecting a relative minimum in the MSLP field, which is essential for pinpointing the core structure of the storm [21,36]. To track the center of Medicanes throughout their relatively short lifespans (typically no more than 2 days at peak development), we use the minimum MSLP values at each grid point in combination with WS data (explained later). Additionally, we performed interpolation on the tracked data to achieve a 30-minute temporal resolution, aligning it with the frequency of satellite observations, specifically Meteosat data. These satellite observations are used to extract various structural characteristics of Medicanes, which will be further discussed in the following section.

Before combining MSLP and WS data to infer the Medicane's trajectories, the events under study (totaling 58) were segmented into two distinct groups, primarily based on their maximum WS values. The first group, referred to as Class 1 or C1, consists of relatively weaker Medicanes with sustained WS ranging from 52 to 81 km/h. The second group, referred to as Class 2 or C2, includes extreme Medicanes, defined by sustained WSs of at least 81 km/h. This categorization facilitated the creation of a binary system, as detailed in Sections 2.3 and 3.2 of this study. It is important to note that approximately 10% of the Medicane cases reported in the literature were excluded from the analysis due to their low intensity, as they exhibited sustained WSs below 52 km/h, which did not meet the criteria for inclusion in our study. The remaining 58 cases were selected because they represent well-documented Medicane events reported in the scientific literature, spanning the period

from 1984 to 2023 (as detailed in Section 3.1). Their selection ensures that the dataset focuses on impactful events with reliable intensity and development characteristics (see, for example, [5,8,9,37]). This selection process was essential due to the lack of a comprehensive Medicane database, requiring reliance on cases already identified in previous studies for training and testing. Additionally, 3 cases from the C2 class underwent further scrutiny in a supplementary experiment (as elaborated in Section 3.2). The complete compilation of Medicane cases is presented in Table 1.

Table 1. Medicane events included in the study. The first column lists the names of each case. The second and third columns display the start and end dates of each cyclone system (D Month YYYY). The last column indicates the class to which each event belongs based on the criteria described in Section 2.1.1.

Storm Name	Beginning Date	Ending Date	Class
Med1984	29 December 1984	31 December 1984	C1
$Med1985_1$	26 October 1985	29 October 1985	C1
$Med1985_2$	13 December 1985	16 December 1985	C1
Med1986	30 September 1986	3 October 1986	C2
Med1989	4 October 1989	6 October 1989	C2
$Med1991_1$	23 November 1991	23 November 1991	C2
$Med1991_2$	6 December 1991	8 December 1991	C2
Med1992	14 October 1992	15 October 1992	C2
Med1994	21 October 1994	25 October 1994	C1
$Med1995_1$	14 January 1995	17 January 1995	C2
$Med1995_2$	27 September 1995	29 September 1995	C1
$Med1996_1$	11 September 1996	13 September 1996	C2
$Med1996_2$ (Cornelia)	6 October 1996	11 October 1996	C2
$Med1996_3$	8 December 1996	11 December 1996	C2
$Med1997_1$	23 September 1997	27 September 1997	C1
$Med1997_2$	28 October 1997	31 October 1997	C2
$Med1997_3$	5 December 1997	8 December 1997	C1
Med1998	25 January 1998	27 January 1998	C2
$Med1999_1$	25 March 1999	28 March 1999	C1
$Med1999_2$	9 December 1999	11 December 1999	C1
$Med1999_3$	19 March 1999	20 March 1999	C1
$Med2000_1$	7 September 2000	9 September 2000	C1
$Med2000_2$	7 October 2000	9 October 2000	C1
Med2001	10 November 2001	12 November 2001	C2
$Med2003_1$	25 May 2003	26 May 2003	C1
$Med2003_2$	17 October 2003	19 October 2003	C2
$Med2004_1$	19 September 2004	20 September 2004	C1
$Med2004_2$	3 November 2004	5 November 2004	C1
$Med2005_1$	13 December 2005	16 December 2005	C2
$Med2005_2$	15 September 2005	16 September 2005	C1
$Med2006_1$	31 January 2006	2 February 2006	C2

Table 1. *Cont.*

Storm Name	Beginning Date	Ending Date	Class
$Med2006_2$	25 September 2006	28 September 2006	C1
$Med2007_1$	15 November 2007	16 November 2007	C2
$Med2007_2$	19 March 2007	22 March 2007	C2
$Med2007_3$	16 October 2007	18 October 2007	C1
$Med2007_4$	25 October 2007	26 October 2007	C2
Med2008	2 December 2008	4 December 2008	C2
Med2009	27 January 2009	29 January 2009	C1
$Med2010_1$	12 October 2010	14 October 2010	C2
$Med2010_2$	2 November 2010	3 November 2010	C1
Med2011 (Rolf)	6 November 2011	9 November 2011	C2
Med2012	13 April 2012	14 April 2012	C2
Med2013	18 November 2013	22 November 2013	C2
$Med2014_1$ (Ilona)	19 January 2014	21 January 2014	C2
$Med2014_2$ (Qendresa)	7 November 2014	8 November 2014	C2
$Med2014_3$	1 December 2014	3 December 2014	C1
Med2016 (Trixie)	29 October 2016	31 October 2016	C1
Med2017 (Numa)	17 November 2017	19 November 2017	C1
Med2018 (Zorbas)	28 September 2018	30 September 2018	C2
$Med2019_1$ (Detlef)	10 November 2019	11 November 2019	C1
$Med2019_2$ (Scott)	24 October 2019	26 October 2019	C1
$Med2020_1$ (Ianos)	15 September 2020	20 September 2020	C2
$Med2020_2$ (Elaina)	14 December 2020	16 December 2020	C1
$Med2020_3$	20 November 2020	24 November 2020	C1
Med2021 (Apollo)	25 October 2021	29 October 2021	C1
$Med2023_1$ (Helios)	20 January 2023	22 January 2023	C1
$Med2023_2$ (Hannelore)	08 February 2023	10 February 2023	C1
$Med2023_3$ (Juliette)	27 February 2023	02 March 2023	C1

Having an equivalent to the International Best Track Archive for Climate Stewardship (IBTrACS) provided by NOAA [38] for the Mediterranean would have been invaluable as a benchmark for comparison, significantly facilitating our analysis. However, only a limited number of referenced studies offer ready-to-use datasets, typically covering a small number of cases with tracking information or other relevant data. These benchmark datasets are often subjectively generated and, therefore, susceptible to potential human error [15]. Moreover, while alternative tracking methodologies for Medicanes exist, they rely on diverse detection techniques and specific thresholds, which produce varying results, as noted by Montella et al. [19]. Given these considerations, direct comparison with satellite data emerges as the most reliable approach currently available for ensuring consistency in tracking and analysis. As a result, we developed our own data collection and tracking framework to build a consistent and reliable dataset. This effort not only ensures robust results for the current study but also provides the scientific community with a curated list of historically relevant Medicanes and their associated structural and temperature features, which can serve as a foundation for future research and model development.

2.1.2. Meteosat Temperature Observations

Due to data availability constraints, we used two different Meteosat imagery products to extract features of the Medicanes' cloud systems for the forecasting analysis. These products, covering the Mediterranean basin, were used to capture snapshots of Medicane events at 30-minute intervals. Between 1984 and 2003, we sourced images from the infrared channel (11.5 µm, 4.5 × 4.5 km pixel size) of the Fundamental Climate Data Record of the Meteosat Visible and Infrared Imager (FCDR MVIRI, https://user.eumetsat.int/s3/eup-strapi-media/C3_S_311b_T4_2_D4_3_MVIRI_FCDR_Release_2_PUG_1b77ce07a9.pdf, accessed on 30 November 2023), while from 2004 onward, data were obtained from channel 9 (10.8 µm, 3 × 3 km pixel size) of the High Rate SEVIRI Level 1.5 Image Data (https://navigator.eumetsat.int/product/EO:EUM:DAT:MSG:HRSEVIRI, accessed on 30 November 2023). Despite the inconsistency in channel wavelength and resolution between the two Meteosat products, there is no significant issue for the application purpose. The features used for forecasting, which capture essential structural and temperature properties of Medicanes, are inherently robust to minor variations in data acquisition methods, such as those introduced by K-means clustering, and remain consistent across different datasets. Additionally, in pattern recognition and machine learning applications, including those using CNNs, models often adapt to data variations during training. This adaptability enables the model to generalize effectively, capturing the relevant patterns and relationships required for accurate forecasting. Therefore, while differences between the data products could theoretically introduce minor discrepancies, their practical impact on the forecasting analysis is expected to be minimal.

To derive Brightness Temperature from pixel counts (FCDR MVIRI) or radiances (SEVIRI), we first conducted a conversion process, followed by the extraction of various features from the observed cloud formations in the images. These parameters—including cloud area, brightness temperature differences between the inner and outer cloud regions, circularity, and eccentricity—were determined using a k-means algorithm to delineate the cloud's edges, following the approach in Martinez-Amaya et al. [29]. The features, calculated at 30-minute intervals, were then aligned with the coordinates obtained from reanalysis data, as discussed in the previous section.

These features are not only extracted at each lead-time but also encompass a temporal dimension, which involves calculating the mean and standard deviation of the temporal variations throughout the entire evolution period of the storm, from its inception to the specified lead-time [25]. Additionally, high-level spatial features, as learned through a CNN method, have been integrated using the methodology outlined in the study conducted by Martinez-Amaya et al. [25].

2.2. Automated Medicane Center Localization

While previous studies have investigated MSLP-based algorithms for tracking Medicanes [10,19], the need for practicality and efficiency calls for the adoption of an automatic methodology, such as the one proposed in this study. It is crucial to note that existing machine learning algorithms were specifically designed to detect the centers of hurricanes and other unique storm types, which possess features and dynamics distinct from Medicanes. Consequently, these algorithms are not well suited for studying Medicanes. Additionally, some of these approaches rely on specific thresholds, such as gradients or distances between track points, which can be arbitrary or dependent on pre-existing labeled data, limiting their general applicability. This underscores the importance of a more adaptable, automated solution. To address this gap, we introduce a novel grid search technique that leverages MSLP data, further enhanced by a k-means algorithm, to localize the centers of Medicanes. Thus, this AI-based approach represents an evolution from existing methods, integrating dynamically adaptive techniques.

In the analysis of each storm, the methodology begins with a grid search for MSLP minima. This process employs a 4.5° × 4.5° sliding window that covers the entire study region for each time step. The selection of this optimal window size was determined through the processing of all available images to ensure accurate detection. Once the

four lowest MSLP points are identified, a 2° × 2° window is applied around each point to run a k-means clustering algorithm. This step segregates the image into two regions, low-pressure and high-pressure areas, and establishes the boundary line between them. Determining this boundary line is instrumental for calculating the circularity of the storm, which reflects the degree of symmetry in its structure [29]. Among the four candidates, we select the one with the highest circularity score, typically indicating a more stable and well-organized cyclonic system. The center of this candidate is then designated as the minimum MSLP center. Subsequently, the maximum WS is identified at each time step, which determines the class of the Medicane, as outlined in Section 2.1. This maximum WS is located within a 4.5° × 4.5° window centered on the calculated MSLP center. However, for the extraction of spatio-temporal features (Section 2.3), a larger 10° × 10° window was used to ensure that the edges of larger storms were fully captured and not missed.

2.3. CNN-RF Model for Medicanes Prediction

Medicanes, which share certain characteristics with tropical cyclones, prompted us to adapt the CNN-RF models developed by Martinez-Amaya et al. [25] to address the unique characteristics of Mediterranean cyclones. Following this methodology, our approach begins with the implementation of a 2D CNN algorithm specifically designed to capture prominent spatial features of the storm cloud system from satellite imagery at various lead-time. Afterward, an RF algorithm is employed to learn these spatial features (extracted from the second-to-last layer of the CNN) in combination with the brightness temperature variables and structural attributes [25]. The goal of this approach is to unveil the nonlinear relationships between the storm characteristics and its potential intensity range. It is important to note that these features indirectly mirror environmental changes [39], leaving distinctive imprints in the size, shape, and temperature characteristics of the storm's cloud system [33,40–43]. Consequently, our method focuses on automatically extracting a unique combination of these properties from satellite images to assess storm intensification. This avoids the need to directly predict based on environmental dynamics or disentangle each individual factor contributing to the Medicane's growth. However, our approach is flexible, allowing for the inclusion of additional variables in future analysis.

For the CNN analysis, we applied a 10° × 10° window to the BT images centered on the coordinates derived from our tracking method (Section 2.2). The images were then resized to 256 × 256 pixels, following the approach outlined by Martinez-Amaya et al. [25]. The decision to use a 256 × 256-pixel receptive field model as a feature extractor was motivated by its proven ability to extract comprehensive features from the images, ensuring that all relevant information is captured within each pixel, as illustrated in Figure 1 (which also presents the CNN layers' architecture). The configuration of the CNN model, including its layers and hyperparameters, was kept consistent with the methodology of Martinez-Amaya et al. [25]. Specifically, the model includes convolutional, max pooling, and fully connected layers to optimize feature extraction and model performance. The rectified linear unit (ReLU) activation function was employed to introduce nonlinearity, enhancing the model's ability to capture complex relationships. Additionally, batch normalization was implemented to expedite training and support more efficient learning. The information extracted from the second-to-last fully connected layer was preserved for later use in the RF algorithm. These features are critical, as they gather high-level data from both the storm and the surrounding environment.

Next, the RF component of our model is trained on all previously mentioned parameters, incorporating their temporal information (see Table 2 for a comprehensive summary of the features used in the final RF classification model). The RF model operates on a binary basis, where prediction accuracy is directly evaluated against actual event occurrences, thus minimizing ambiguity in performance assessment and providing a straightforward measure of forecasting reliability without requiring complex model-to-model comparisons [25]. This model effectively differentiates between the two predefined classes of Medicanes, C1, and C2, predicting the most likely class for each event based on distinctive storm

cloud characteristics, even days before reaching peak WS intensity. This approach ensures robustness by focusing on the most distinctive patterns associated with the majority of events, minimizing the impact of isolated cases that may be misclassified due to the spatial resolution limitations of the WS product. Additionally, a thorough prior review of all cases was conducted to verify that the maximum WS, critical for determining storm classification, aligned with reported values, ensuring accurate categorization of each event. To further ensure robustness, we implemented a 5-fold cross-validation strategy, with each fold using 80% of the data for training and the remaining 20% for testing [25]. For each lead-time, we evaluated the mean and standard deviation across the five trained models, with a focus on precision within the extreme class (p_{C2}), calculated relative to the total number of actual extreme occurrences, as our primary goal was to predict events with the potential for the most severe impacts [25]. The RF algorithm's design thus promotes reliability through rigorous validation against test data throughout training. Additionally, in a separate experiment presented in Section 3, we evaluated rapidly developing C2 cases using the hit ratio, a statistical measure that calculates the percentage of correctly predicted events relative to the total number of actual events [25].

Table 2. Overview of input variables incorporated into the RF algorithm for extreme Medicane forecasting. The first column enumerates the variable names, while the second column furnishes their corresponding descriptions. The storm cloud contours were delineated using a K-means algorithm (detailed by Martinez-Amaya et al. [29]), facilitating the derivation of the first four features for each event. Four additional inputs offer temporal insights associated with these variables. This temporal dimension (t) represents the mean and standard deviation of the time range from TC formation to a specified lead-time. The last input corresponds to the high-level spatial features acquired through the CNN method. The model encompasses a total of nine input variables: A, ΔT, C, ε, A_t, ΔT_t, C_t, ε_t, and CNN.

Variable Name	Description
Area (A)	Size of the storm cloud in km^2
TempDiff (ΔT)	Temperature difference between the outer part and the inner core of the storm cloud in °C
Circularity (C)	Feature representing the symmetry of the storm cloud (unit-free)
Eccentricity (ε)	Feature representing the eccentricity of the storm cloud (unit-free)
HSF CNN (CNN)	High-level spatial feature extracted using the CNN algorithm applied to a $10^\circ \times 10^\circ$ window around the storm's center in °C

It is important to note that we chose RF as the final classifier instead of a CNN due to its higher reliability in situations with limited dataset availability and its superior handling of overfitting, as noted by Kwak et al. [44] and Martinez-Amaya et al. [25]. Following Martinez-Amaya et al. [25], we restricted each model to a maximum of 100 trees and implemented a stopping criterion along with regularization terms to optimize performance and minimize overfitting risks. To enhance classification accuracy, we explored two distinct data configurations: a balanced dataset (BD), created by randomly undersampling the majority class as per Martinez-Amaya et al. [25], and an all-data (AD) configuration, which uses the entire dataset with a focus on error penalization in the minority class. Prioritizing error penalization for the minority class is crucial when using the full dataset, as models can otherwise disproportionately learn patterns from the majority class, leading to the misclassification of the critical minority class [45], which often holds greater significance [46,47]. To address this, we introduced a cost-sensitive approach inspired by Li et al. [46] and Dablain et al. [48], applying higher penalties for misclassifying minority class events. For example, with 20 C1 events and 10 C2 events, we doubled the penalty for misclassifying C2 events. We further tested both data configurations (BD and AD) with and without data augmentation to assess potential performance improvements from expanding the dataset. Data augmentation was achieved through rotations (90°, 180°, and 270°) and flipping (hori-

zontally and vertically) [25,49]. This approach allowed us to assess the model's adaptability and effectiveness in scenarios with augmented event counts.

Figure 1. Illustration of high-level spatial features (feature maps) extracted by the CNN, showcasing the learning process across various CNN layers for specific events: (**a**) Medicane Ianos (6 h lead-time); (**b**) Medicane Numa (18 h lead-time). Each image represents the mean value of all the filters considered within each layer. The size, number of filters, and type of layer used are denoted as follows: Layer (sizeX, sizeY, #filters). 'Conv' stands for Convolutional, 'MaxPool' for Max Pooling, 'BN' for Batch Normalization, 'DO' for Dropout, and 'FC' for Fully Connected layers. Note that the convolutional layers capture key features through adaptive kernel filters, the max pooling layer condenses important information, and the fully connected layers prepare the output for classification. The hyperparameter values and regularization terms, including dropout, were adopted from the best-performing model presented in Martinez-Amaya et al. [25]. Refer to Yamashita et al. [50] for comprehensive insights into CNN architecture and the training for learning high-level spatial features.

3. Results and Discussion

Within the subsequent segment, we engage in a detailed discussion of our findings. The results shed light on the performance of our tracking and forecasting models and their implications for understanding and predicting Medicane phenomena.

3.1. Insights into Medicanes Tracking

As outlined in Section 2.2, our tracking methodology integrates both WS and MSLP reanalysis data using their respective maximum and minimum values. This process is enhanced by a k-means algorithm, which facilitates the identification of the storm's center throughout its entire lifespan. The inclusion of the k-means algorithm is essential, as the presence of other weather systems in the Mediterranean Sea region can lead to inaccuracies in estimating the event's exact location. By employing k-means, we can delineate the boundaries of the storm, assess its symmetry (circularity), and distinguish the cyclonic system from other weather systems. This significantly improves our ability to pinpoint the center of Medicanes for tracking purposes.

Given the lack of available ground-truth tracking data for Medicanes, a quantitative comparative analysis was not feasible. To address this limitation, we implemented a rigorous visual inspection process using multiple reference products, including BT satellite imagery, MSLP, and WS fields, which provide a reliable basis for visually identifying the storm's center (see Section 2.1). This approach allowed us to assess the alignment between the visually identified storm center and the center predicted by our model, indicated by a cross in Figure 2. Although detailed figures for all 58 analyzed cases are impractical to include, we provide two illustrative examples in Figure 2: the events of Numa (a non-extreme cyclone in 2017) and Ianos (an extreme cyclone from 2020).

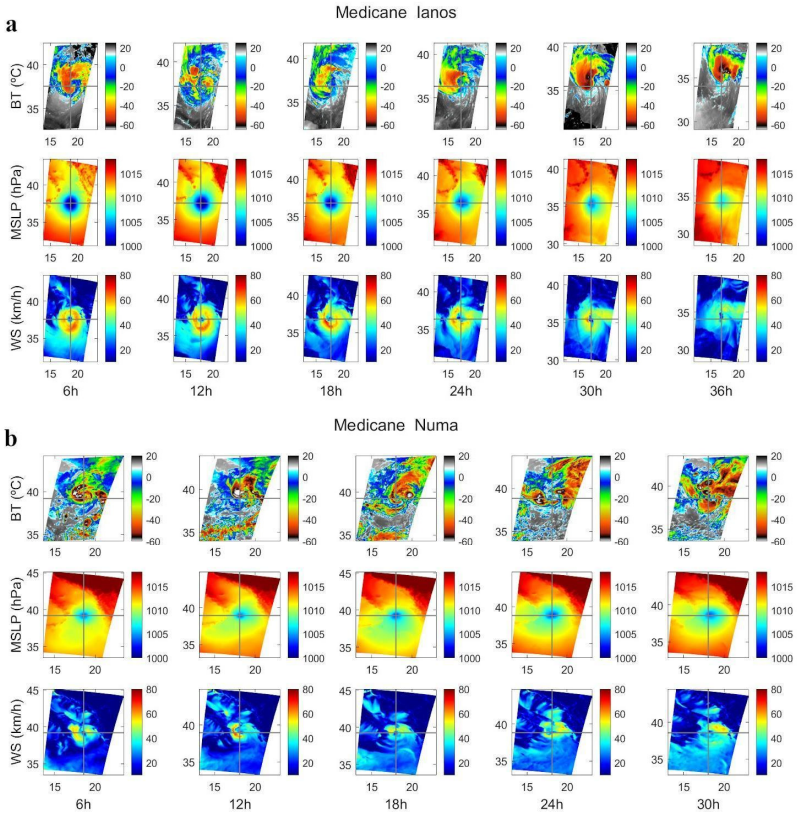

Figure 2. Track analysis of Medicanes Ianos (**a**) and Numa (**b**). For both cases, moving from left to right, the first two rows present BT images (in °C) and MSLP maps (in hPa), respectively, at 6, 12, 18, 24, 30 h (and 36 h, for Ianos) preceding the peak WS. The bottom row displays the same temporal data but for WS maps (in km/h). In all plots, a gray cross is depicted, centered at the latitude and longitude of the Medicane center, calculated using the methodology outlined in Section 2.2.

As expected, as a Medicane intensifies (from 30 h to its peak at 0 h), the storm's center becomes more discernible due to increased symmetry in the storm structure, underscoring the robustness of our tracking methodology. However, minor misplacements of the center may occasionally occur, especially during phases of temporary weakening before the storm regains strength (as seen in the Ianos case, 12 h before its peak in Figure 2a) or when the storm is still distant from peak intensity (as in the Numa case, 30 h before its peak in Figure 2b). It is also worth noting that the limited spatial resolution of the reanalysis data (~31 km), particularly post-2020, may affect center tracking accuracy due to potential alignment discrepancies. Despite these limitations, our method establishes a solid foundation for Medicane tracking, with the potential for even greater accuracy as higher-resolution and standardized datasets become available. The implications of these findings for forecasting accuracy are further explored in the following section.

3.2. Exploring CNN-RF Predictions for Extreme Medicanes

Here, we present and discuss the outcomes of our CNN-RF model's predictions on a dataset comprising 58 Mediterranean cyclones, used for both training and testing (see Section 2.3 for details on the model configuration). As mentioned earlier, the RF-based forecasting system provides reliable binary outcomes for C2 Medicanes, where the accuracy of each forecast can be directly confirmed or denied based on actual event occurrences (see Section 2.1). Figure 3 provides an overview of the model's precision for the C2 class across all lead-time and various tests described in Section 2.3. The lead-time represent prediction intervals (every 6 h) from the time the prediction is made (when all predictors are inferred) up to the event's peak development (see Section 2.3 for more details). Predictions are generated within a 6- to 36-hour window prior to the event's peak WS, as data beyond 36 h are insufficient for deep learning modeling. As outlined in Section 2.3, the model's predictions rely on the spatio-temporal characteristics of cloud formations along the tracking trajectory identified in the preceding experiment. We conducted four distinct tests (see Section 2.3): (1) balanced dataset (BD); (2) balanced dataset with data augmentation (BD with DA); (3) all dataset (AD); and (4) all dataset with data augmentation (AD with DA). The number of available cases for each lead-time is shown, along with the final count when data augmentation is applied. The results indicate that the AI model predicts extreme Medicanes (C2 class) with precision consistently exceeding at least 60% at lead-time beyond 24 h, presenting a promising approach for the early prediction of these severe weather events (see Figure 3).

The approach using all available data with data augmentation emerged as the most stable model across all lead-time. As expected, in cases with fewer available events, data augmentation proved crucial, particularly for extended lead-time. However, it should be noted that data augmentation can introduce challenges, such as amplifying errors when dealing with tracking data that may contain bias [51]. To mitigate these issues, it is essential to prioritize model error weighting over event loss in cases of data imbalance (see Section 2.3). This approach ensures that all available cases are preserved, allowing the model to account for a wide range of scenarios during training, which in turn leads to a more realistic forecast assessment. The mean precision across all lead-time is approximately 71%, reaching a peak of 80% at the 36 h mark (with 13 cases). In cases where storms exhibit less distinguishable features between group classes, the reduced precision for intermediate states is expected, albeit still above 65%, as shown in Figure 3. As lead-time approach the event peak, the influence of undersampling or data augmentation strategies diminishes due to the relatively higher number of available events for the model to make accurate predictions using a balanced dataset.

Finally, to further evaluate the effectiveness of our predictive models, we conducted an additional analysis focusing on three challenging cases of rapid intensification—Med1991, $Med2010_1$, and $Med2014_2$—all categorized as C2 storms. This evaluation used the Hit Ratio (HR) metric (see Section 2.3) and was conducted with the best-performing forecasting model (i.e., AD with DA). The final class of both extreme Med1991 and $Med2010_1$ Medicanes

was successfully predicted by at least four out of the five models across all lead-time, with HR values of 80% or higher. This accuracy was maintained despite the rapidly evolving features within an 18 h window and significant variations in intensification rates (ranging from 44 km/h to 115 km/h and from 56 km/h to 87 km/h, respectively), demonstrating the robustness of the model. The tracking results of the studied Medicanes, which originated on 23 November 1991 off the Eastern Tunisian coast and on 12 October 2010 near the Balearic Islands region, are illustrated in Figure 4. The predictability of Med2014$_2$, which originated in the Ionian Sea on 5 November 2014, posed significant challenges for numerical weather models due to inaccuracies in initial conditions and the complex mesoscale dynamics driving its rapid intensification [52]. Yet, our model successfully predicted its intensification to severe status, achieving an increase in HR values from 60% to 80% as it evolved toward its peak intensity (from approximately 68 km/h to 97 km/h in less than 12 h), as shown in Figure 4.

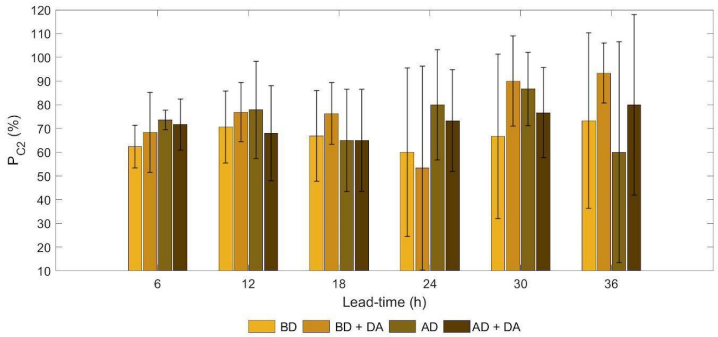

Lead-time (h)	6h	12h	18h	24h	30h	36h
# Samples C1 (DA)	29 (144)	24 (119)	21 (106)	16 (81)	13 (63)	10 (50)
# Samples C2 (DA)	29 (144)	24 (119)	18 (88)	12 (57)	9 (44)	3 (13)

Figure 3. Prediction precision for C2 Medicanes across all model experiments. Displayed from left to right are results for the BD, BD with DA, AD, and AD with DA approaches. The error bar in the figure represents the standard deviation derived from the 5-fold cross-validation models (see Section 2.3). The table below shows the initial number of cases, denoted as '# Samples' for each class before random undersampling or the application of DA. This is denoted in parentheses when DA is applied.

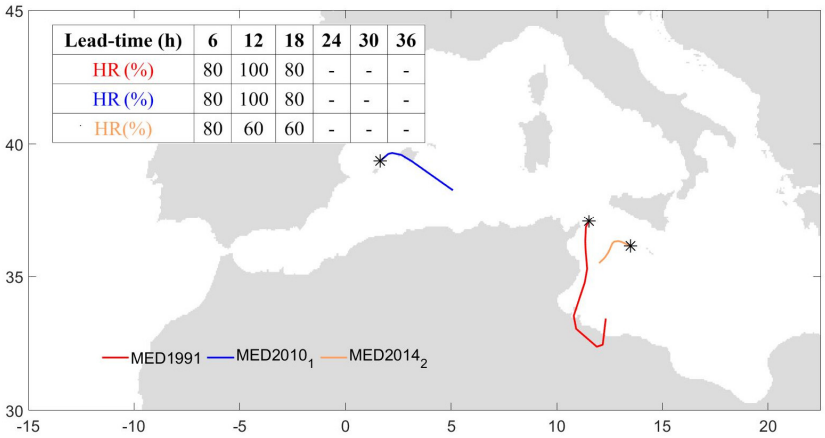

Figure 4. Trajectories generated from the point of origin to their maximum WS (indicated with an asterisk) for Medicanes Med1991, Med2010$_1$, and Med2014$_2$, along with HR analysis results from the most robust model approach (i.e., AD with DA). HR values are provided only from an 18 h lead-time onward due to the short duration of the events analyzed.

4. Conclusions

Medicanes are cyclones in the Mediterranean region that, according to the IPCC report, are likely to intensify due to climate change. To effectively monitor and predict these hazards, it is essential to develop advanced, adaptable models that can track their paths and identify early warning signals that capture intensifying features of cyclonic development. This work contributes to the growing field of AI applications in climate research by demonstrating the adaptability of machine learning techniques for tracking and forecasting Mediterranean cyclones. It provides a rapid, efficient alternative to traditional, resource-intensive models, offering valuable insights into these extreme weather events that are crucial for building climate resilience.

The initial step in the proposed AI framework involved developing an automated tracking technique that uses a k-means algorithm alongside reanalysis data to map the trajectories of the most documented Medicanes. Although automated, the tracking system's accuracy is validated through rigorous visual verification against high-resolution Meteosat images, which provides an essential quality check in the absence of a reliable, unified, and objective benchmark dataset for Medicanes. Despite current limitations due to the restricted spatio-temporal resolution of reanalysis data—which is updated on a weekly to seasonal basis—the model's robustness and adaptability highlight its strong potential for achieving even greater precision as higher-resolution data become available. Nevertheless, our approach demonstrates that the use of different reanalysis products does not critically impact the forecasting analysis. By focusing on relative MSLP and WS values rather than their absolute ones, we ensure consistent identification of Medicane features despite differences in data resolution. Furthermore, the use of sliding windows (e.g., $4.5^\circ \times 4.5^\circ$ for MSLP minima tracking and $10^\circ \times 10^\circ$ for feature extraction) enables robust detection of key storm characteristics, effectively accommodating variability in spatial resolution across datasets. This enhancement positions our AI framework as a valuable addition to early warning systems, capable of advancing Medicane monitoring in future applications.

In the second phase, we tailored a CNN-RF model, an AI technique designed to capture the complex, nonlinear relationships between spatio-temporal storm information from satellite imagery (key structural cyclonic features) and the peak intensity of Medicane events, enabling predictions of extreme Medicanes. Our most robust model consistently achieves a precision rate of 65% or higher, depending on storm duration and forecast lead-time, with the highest precision reaching 80% for forecasts made 36 h in advance. We also address the challenges posed by imbalanced and limited data scenarios, highlighting the importance of retaining all events and employing data augmentation techniques. The case studies on rapid intensification demonstrate the model's ability to generalize effectively, even in challenging scenarios.

In conclusion, our study marks a significant advancement in understanding and predicting Mediterranean cyclones, showcasing the potential of AI-based approaches to support forecasting in the context of a changing climate. The approach establishes a new benchmark, facilitating cross-analysis with other methodologies and offering a deeper understanding of Medicanes, particularly in the absence of reference datasets. This study not only advances our understanding of Medicanes but also contributes a scalable AI-based tool that could be adapted to predict and mitigate the impacts of other climate-related extreme events as they become more frequent and severe under climate change scenarios. We encourage further exploration of additional storm growth variables to mitigate the potential impacts of these natural disasters.

Author Contributions: Conceptualization: V.N.; Methodology: V.N., J.M.-A. and J.M.-M.; Investigation: V.N. and J.M.-A.; Analysis, Validation, and Data Curation: J.M.-A. and V.N.; Visualization: J.M.-A. and V.N.; Writing—Original Draft Preparation: J.M.-A.; Writing—Review and Editing: V.N. and J.M.-A.; Supervision: V.N.; Funding Acquisition, Resources, and Project Administration: V.N. All authors have read and agreed to the published version of the manuscript.

Funding: This research was funded by the European Space Agency (contract 4000134529/21/NL/GLC/my), the Ministry of Culture, Education, and Science of the Generalitat Valenciana (grant CIDEGENT/2019/055), and the Spanish Ministry of Science and Innovation through the European Union NextGenerationEU (PRTR-C17.I1) and the Generalitat Valenciana (GVA-THINKINAZUL/2021/018).

Data Availability Statement: The datasets generated for this study can be found in the AI4OCEANS repository (https://github.com/AI4OCEANS/, accessed on 30 November 2023).

Acknowledgments: The authors gratefully acknowledge the computer resources at Artemisa, funded by the European Union ERDF and Comunitat Valenciana.

Conflicts of Interest: The authors declare no conflicts of interest. The funders had no role in the design of the study; in the collection, analyses, or interpretation of data; in the writing of the manuscript; or in the decision to publish the results.

References

1. Bhatia, K.T.; Vecchi, G.A.; Knutson, T.R.; Murakami, H.; Kossin, J.; Dixon, K.W.; Whitlock, C.E. Recent increases in tropical cyclone intensification rates. *Nat. Commun.* **2020**, *10*, 1–9. [CrossRef]
2. Hicke, J.A.; Lucatello, S.; Mortsch, L.D.; Dawson, J.; Aguilar, M.D.; Enquist, C.A.F. North America. In *Climate Change 2022: Impacts, Adaptation and Vulnerability*; Contribution of Working Group II to the Sixth Assessment Report of the Intergovernmental Panel on Climate, Change; Pörtner, H.-O., Roberts, D.C., Tignor, M.M.B., Poloczanska, E., Mintenbeck, K., Alegría, A., Craig, M., Langsdorf, S., Löschke, S., Möller, V., et al., Eds.; Cambridge University: Cambridge, UK; New York, NY, USA, 2022; pp. 1929–2042.
3. Koseki, S.; Mooney, P.A.; Cabos, W.; Gaertner, M.; de la Vara, A.; González-Alemán, J.J. Modelling a tropical-like cyclone in the Mediterranean Sea under present and warmer climate. *Nat. Hazards Earth Syst. Sci.* **2021**, *21*, 53–71. [CrossRef]
4. Pytharoulis, I. Analysis of a Mediterranean tropical-like cyclone and its sensitivity to the sea surface temperatures. *Atmospheric Res.* **2018**, *208*, 167–179. [CrossRef]
5. Dafis, S.; Claud, C.; Kotroni, V.; Lagouvardos, K.; Rysman, J. Insights into the convective evolution of Mediterranean tropical-like cyclones. *Q. J. R. Meteorol. Soc.* **2020**, *146*, 4147–4169. [CrossRef]
6. Lagouvardos, K.; Karagiannidis, A.; Dafis, S.; Kalimeris, A.; Kotroni, V. Ianos—A Hurricane in the Mediterranean. *Bull. Am. Meteorol. Soc.* **2021**, *103*, E1621–E1636. [CrossRef]
7. Di Muzio, E.; Riemer, M.; Fink, A.H.; Maier-Gerber, M. Assessing the predictability of Medicanes in ECMWF ensemble forecasts using an object-based approach. *Q. J. R. Meteorol. Soc.* **2019**, *145*, 1202–1217. [CrossRef]
8. Nastos, P.; Papadimou, K.K.; Matsangouras, I. Mediterranean tropical-like cyclones: Impacts and composite daily means and anomalies of synoptic patterns. *Atmospheric Res.* **2018**, *208*, 156–166. [CrossRef]
9. Portmann, R.; González-Alemán, J.J.; Sprenger, M.; Wernli, H. How an uncertain short-wave perturbation on the North Atlantic wave guide affects the forecast of an intense Mediterranean cyclone (Medicane Zorbas). *Weather. Clim. Dyn.* **2020**, *1*, 597–615. [CrossRef]
10. Pravia-Sarabia, E.; Gómez-Navarro, J.J.; Jiménez-Guerrero, P.; Montávez, J.P. TITAM (v1.0): The Time-Independent Tracking Algorithm for Medicanes. *Geosci. Model Dev.* **2020**, *13*, 6051–6075. [CrossRef]
11. González-Alemán, J.J.; Pascale, S.; Gutierrez-Fernandez, J.; Murakami, H.; Gaertner, M.A.; Vecchi, G.A. Potential Increase in Hazard From Mediterranean Hurricane Activity With Global Warming. *Geophys. Res. Lett.* **2019**, *46*, 1754–1764. [CrossRef]
12. Ali, E.; Cramer, W.; Carnicer, J.; Georgopoulou, E.; Hilmi, N.J.M.; Cozannet, G.L.; Lionello, P. Cross-Chapter Paper 4: Mediterranean Region. In *Climate Change 2022: Impacts, Adaptation and Vulnerability*; Contribution of Working Group II to the Sixth Assessment Report of the Intergovernmental Panel on Climate, Change; Pörtner, H.-O., Roberts, D.C., Tignor, M.M.B., Poloczanska, E., Mintenbeck, K., Alegría, A., Craig, M., Langsdorf, S., Löschke, S., Möller, V., et al., Eds.; Cambridge University: Cambridge, UK; New York, NY, USA, 2022; pp. 2233–2272.
13. Romero, R.; Emanuel, K. Medicane risk in a changing climate. *J. Geophys. Res. Atmos.* **2013**, *118*, 5992–6001. [CrossRef]
14. Flaounas, E.; Davolio, S.; Raveh-Rubin, S.; Pantillon, F.; Miglietta, M.M.; Gaertner, M.A.; Hatzaki, M.; Homar, V.; Khodayar, S.; Korres, G.; et al. Mediterranean cyclones: Current knowledge and open questions on dynamics, prediction, climatology and impacts. *Weather. Clim. Dyn.* **2022**, *3*, 173–208. [CrossRef]
15. Flaounas, E.; Aragão, L.; Bernini, L.; Dafis, S.; Doiteau, B.; Flocas, H.; Gray, S.L.; Karwat, A.; Kouroutzoglou, J.; Lionello, P.; et al. A composite approach to produce reference datasets for extratropical cyclone tracks: Application to Mediterranean cyclones. *Weather. Clim. Dyn.* **2023**, *4*, 639–661. [CrossRef]
16. Dafis, S.; Rysman, J.; Claud, C.; Flaounas, E.; Dafis, S.; Rysman, J.; Claud, C.; Flaounas, E.; Dafis, S.; Rysman, J.; et al. Remote sensing of deep convection within a tropical-like cyclone over the Mediterranean Sea. *Atmospheric Sci. Lett.* **2018**, *19*. [CrossRef]
17. Menna, M.; Martellucci, R.; Reale, M.; Cossarini, G.; Salon, S.; Notarstefano, G.; Mauri, E.; Poulain, P.-M.; Gallo, A.; Solidoro, C. A case study of impacts of an extreme weather system on the Mediterranean Sea circulation features: Medicane Apollo (2021). *Sci. Rep.* **2023**, *13*, 1–15. [CrossRef]
18. Tous, M.; Romero, R. Meteorological environments associated with medicane development. *Int. J. Clim.* **2012**, *33*, 1–14. [CrossRef]

19. Montella, R.; Di Luccio, D.; Ciaramella, A.; Foster, I. StormSeeker: A Machine-Learning based Mediterranean storm tracer. In *Internet and Distributed Computing Systems*; Montella, R., Ciaramella, A., Fortino, G., Guerrieri, A., Liotta, A., Eds.; Springer: Cham, Switzerland, 2019; Volume 11874, pp. 444–456. [CrossRef]
20. Cavicchia, L.; von Storch, H.; Gualdi, S. A long-term climatology of medicanes. *Clim. Dyn.* **2013**, *43*, 1183–1195. [CrossRef]
21. Picornell, M.A.; Campins, J.; Jansà, A. Detection and thermal description of medicanes from numerical simulation. *Nat. Hazards Earth Syst. Sci.* **2014**, *14*, 1059–1070. [CrossRef]
22. Listowski, C.; Forestier, E.; Dafis, S.; Farges, T.; De Carlo, M.; Grimaldi, F.; Le Pichon, A.; Vergoz, J.; Heinrich, P.; Claud, C. Remote Monitoring of Mediterranean Hurricanes Using Infrasound. *Remote. Sens.* **2022**, *14*, 6162. [CrossRef]
23. Romero, R. A method for quantifying the impacts and interactions of potential-vorticity anomalies in extratropical cyclones. *Q. J. R. Meteorol. Soc.* **2008**, *134*, 385–402. [CrossRef]
24. Jourdan, A.; Loubière, P. *Sensitivity Analysis in TORUS 1 –Toward an Open Resource Using Services*; Laffly, D., Ed.; John Wiley & Sons, Ltd: New York, NY, USA, 2020; pp. 107–128. [CrossRef]
25. Martinez-Amaya, J.; Longépé, N.; Nieves, V.; Muñoz-Marí, J. Improved forecasting of extreme hurricane events by integrating spatio-temporal CNN-RF learning of tropical cyclone characteristics. *Front. Earth Sci.* **2023**, *11*, 1223154. [CrossRef]
26. Cangialosi, J.P.; Blake, E.; DeMaria, M.; Penny, A.; Latto, A.; Rappaport, E.; Tallapragada, V. Recent Progress in Tropical Cyclone Intensity Forecasting at the National Hurricane Center. *Weather. Forecast.* **2020**, *35*, 1913–1922. [CrossRef]
27. Nystrom, R.G.; Zhang, F. Practical Uncertainties in the Limited Predictability of the Record-Breaking Intensification of Hurricane Patricia (2015). *Mon. Weather. Rev.* **2019**, *147*, 3535–3556. [CrossRef]
28. Gupta, U.; Jitkajornwanich, K.; Elmasri, R.; Fegaras, L. Adapting K-means clustering to identify spatial patterns in storms. In Proceedings of the 2016 IEEE International Conference on Big Data (Big Data), Washington, DC, USA, 5–8 December 2016; pp. 2646–2654.
29. Martinez-Amaya, J.; Radin, C.; Nieves, V. Advanced Machine Learning Methods for Major Hurricane Forecasting. *Remote. Sens.* **2022**, *15*, 119. [CrossRef]
30. Maskey, M.; Ramachandran, R.; Ramasubramanian, M.; Gurung, I.; Freitag, B.; Kaulfus, A.; Bollinger, D.; Cecil, D.J.; Miller, J. Deepti: Deep-Learning-Based Tropical Cyclone Intensity Estimation System. *IEEE J. Sel. Top. Appl. Earth Obs. Remote. Sens.* **2020**, *13*, 4271–4281. [CrossRef]
31. Carmo, A.R.; Longepe, N.; Mouche, A.; Amorosi, D.; Cremer, N. Deep Learning Approach for Tropical Cyclones Classification Based on C-Band Sentinel-1 SAR Images. In Proceedings of the IGARSS 2021–2021 IEEE International Geoscience and Remote Sensing Symposium, Brussels, Belgium, 11–16 July 2021; pp. 3010–3013.
32. Asif, A.; Dawood, M.; Jan, B.; Khurshid, J.; DeMaria, M.; Minhas, F.U.A.A. PHURIE: Hurricane intensity estimation from infrared satellite imagery using machine learning. *Neural Comput. Appl.* **2018**, *32*, 4821–4834. [CrossRef]
33. Song, J.; Duan, Y.; Klotzbach, P.J. Revisiting the Relationship Between Tropical Cyclone Size and Intensity Over the Western North Pacific. *Geophys. Res. Lett.* **2020**, *47*. [CrossRef]
34. Schimanke, S.; Ridal, M.; Le Moigne, P.; Berggren, L.; Undén, P.; Randriamampianina, R.; Andrea, U.; Bazile, E.; Bertelsen, A.; Brousseau, P.; et al. CERRA sub-daily regional reanalysis data for Europe on single levels from 1984 to present. Copernicus Climate Change Service (C3S) Climate Data Store (CDS). 2021. Available online: https://cds.climate.copernicus.eu/datasets/reanalysis-cerra-single-levels?tab=overview (accessed on 30 November 2023).
35. Hersbach, H.; Bell, B.; Berrisford, P.; Biavati, G.; Horányi, A.; Muñoz Sabater, J.; Nicolas, J.; Peubey, C.; Radu, R.; Rozum, I.; et al. ERA5 Hourly Data on Single Levels from 1979 to Present. Copernicus Climate Change Service (C3S) Climate Data Store (CDS). 2018. Available online: https://cds.climate.copernicus.eu/datasets/reanalysis-era5-single-levels?tab=overview (accessed on 30 November 2023).
36. Zhang, W.; Villarini, G.; Scoccimarro, E.; Napolitano, F. Examining the precipitation associated with medicanes in the high-resolution ERA-5 reanalysis data. *Int. J. Clim.* **2020**, *41*, E126–E132. [CrossRef]
37. Ferrarin, C.; Pantillon, F.; Davolio, S.; Bajo, M.; Miglietta, M.M.; Avolio, E.; Carrió, D.S.; Pytharoulis, I.; Sanchez, C.; Patlakas, P.; et al. Assessing the coastal hazard of Medicane Ianos through ensemble modelling. *Nat. Hazards Earth Syst. Sci.* **2023**, *23*, 2273–2287. [CrossRef]
38. Knapp, K.R.; Kruk, M.C.; Levinson, D.H.; Diamond, H.J.; Neumann, C.J. The International Best Track Archive for Climate Stewardship (IBTrACS): Unifying tropical cyclone best track data. *Bull. Am. Meteorol. Soc.* **2010**, *91*, 363–376. [CrossRef]
39. Zehr, R.M. Environmental Vertical Wind Shear with Hurricane Bertha (1996). *WAF* **2003**, *18*, 345–356. [CrossRef]
40. Wu, L.; Tian, W.; Liu, Q.; Cao, J.; Knaff, J.A. Implications of the Observed Relationship between Tropical Cyclone Size and Intensity over the Western North Pacific. *J. Clim.* **2015**, *28*, 9501–9506. [CrossRef]
41. Guo, X.; Tan, Z. Tropical cyclone fullness: A new concept for interpreting storm intensity. *Geophys. Res. Lett.* **2017**, *44*, 4324–4331. [CrossRef]
42. Xu, J.; Wang, Y. Dependence of Tropical Cyclone Intensification Rate on Sea Surface Temperature, Storm Intensity, and Size in the Western North Pacific. *Weather. Forecast.* **2018**, *33*, 523–537. [CrossRef]
43. Chen, K.; Chen, G.; Rao, C.; Wang, Z. Relationship of tropical cyclone size change rate with size and intensity over the western North Pacific. *Atmospheric Ocean. Sci. Lett.* **2021**, *14*. [CrossRef]
44. Kwak, G.-H.; Park, C.-W.; Lee, K.-D.; Na, S.-I.; Ahn, H.-Y.; Park, N.-W. Potential of Hybrid CNN-RF Model for Early Crop Mapping with Limited Input Data. *Remote. Sens.* **2021**, *13*, 1629. [CrossRef]

45. Johnson, J.M.; Khoshgoftaar, T.M. Survey on deep learning with class imbalance. *J. Big Data* **2019**, *6*, 27. [CrossRef]
46. Li, Q.; Zhao, C.; He, X.; Chen, K.; Wang, R. The Impact of Partial Balance of Imbalanced Dataset on Classification Performance. *Electronics* **2022**, *11*, 1322. [CrossRef]
47. Joloudari, J.H.; Marefat, A.; Nematollahi, M.A.; Oyelere, S.S.; Hussain, S. Effective Class-Imbalance Learning Based on SMOTE and Convolutional Neural Networks. *Appl. Sci.* **2023**, *13*, 4006. [CrossRef]
48. Dablain, D.; Jacobson, K.N.; Bellinger, C.; Roberts, M.; Chawla, N.V. Understanding CNN fragility when learning with imbalanced data. *Mach. Learn.* **2023**, *113*, 4785–4810. [CrossRef]
49. Mumuni, A.; Mumuni, F. Data augmentation: A comprehensive survey of modern approaches. *Array* **2022**, *16*. [CrossRef]
50. Yamashita, R.; Nishio, M.; Do, R.K.G.; Togashi, K. Convolutional neural networks: An overview and application in radiology. *Insights Imaging* **2018**, *9*, 611–629. [CrossRef] [PubMed]
51. Shorten, C.; Khoshgoftaar, T.M. A survey on Image Data Augmentation for Deep Learning. *J. Big Data* **2019**, *6*, 60. [CrossRef]
52. Carrió, D.S. Improving the predictability of the Qendresa Medicane by the assimilation of conventional and atmospheric motion vector observations. Storm-scale analysis and short-range forecast. *Nat. Hazards Earth Syst. Sci.* **2023**, *23*, 847–869. [CrossRef]